Boosting the Photoactivity of Grafted Titania: Ultrasound-Driven Synthesis of a Multi-Phase Heterogeneous Nano-Architected Photocatalyst

Dimitrios A. Giannakoudakis[1,2]*, *Abdul Qayyum*[1], *Dariusz Łomot*[1], *Maximilian Besenhard*[3], *Dmytro Lisovytskiy*[1], *Teresa J. Bandosz*[2]*, *Juan Carlos Colmenares*[1]*

[1] Institute of Physical Chemistry, Polish Academy of Sciences, Kasprzaka 44/52, 01-224, Warsaw, Poland

[2] Department of Chemistry and Biochemistry, The City College of New York, New York, NY, USA

[3] Department of Chemical Engineering, University College London, Torrington Place, London, UK 10031

*Corresponding authors' emails: DaGchem@gmail.com (DAG), tbandosz@ccny.cuny.edu (TJB), jcarloscolmenares@ichf.edu.pl (JCC)

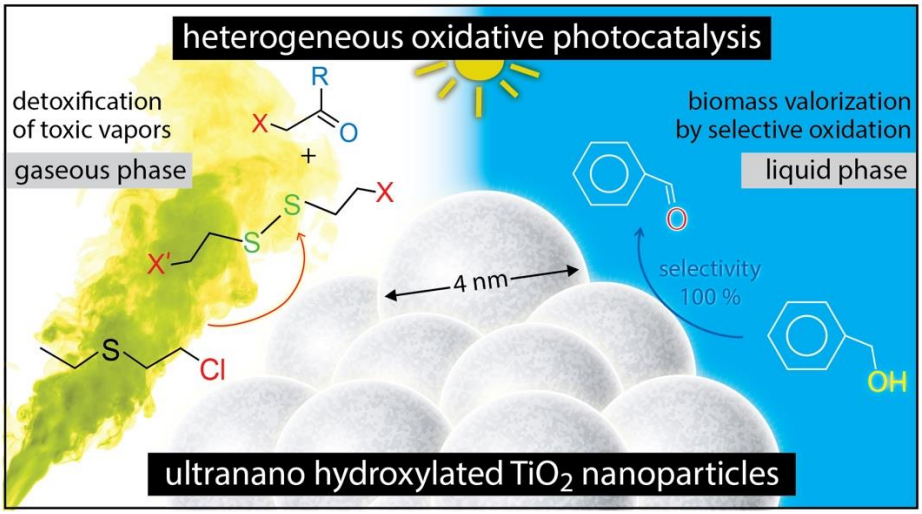

Keywords: heterogeneous photocatalysis, ultrasound assisted synthesis, titanium oxide nanoparticles, chemical warfare agents, biomass valorization

Abstract - 150 words maximum

The utilization of mechanochemistry, and specifically of ultrasonication, can arise new opportunities on the design and synthesis in materials chemistry, and more interestingly of novel nano-photocatalysts. Herein, a low-power high-frequency (500 kHz) ultrasound-assisted precipitation synthesis (LPHFUS) led to a unique multiphase nano-structured titanium dioxide of a high surface area (326 m^2/g), total pores volume (0.484 cm^3/g) and enhanced surface chemistry heterogeneity. The design of this synthetic protocol avoids the energy demanding step of calcination for crystallization, while utilizes the organic residues towards the introduction of various surface carbon/oxygen containing functionalities(JC: If we are convinced (with strong evidence) how those functionalities were formed (the whole mechanism of our material synthesis) then I think we have some chances in Nature Materials) and to control the anatase nanocrystals (4 to 7 nm in size) surrounded by an amorphous titanium hydroxide network. This nanomaterial showed a superior performance as a heterogenous photocatalyst either in a gaseous phase against toxic vapors of chemical warfare agents (a mustard gas surrogate), or in liquid phase, for the selective oxidation of benzyl alcohol, a model lignin-biomass derived compound.

Introduction

An essential and “green” aspect of environmental sustainability is the utilization of the abundant and naturally available source of power, sunlight. After an innovative announcement of Fujishima and Honda (1972) on utilizing TiO_2 as a semiconductor photocatalyst for the photo-electro-catalytic water splitting,[1] heterogeneous photocatalysis have been widely used also for

environmental remediation and in organic synthetic chemistry.[2–4] Nevertheless, its vital disadvantage (JC: disadvantage? If we are thinking about AOP: the main goal is to mineralize everything organic (no selectivity)) is that the advanced oxidation processes (AOPs), which provide a high reactivity, are nonselective, especially in aqueous media.[5–9] A design and synthesis of an efficient photocatalyst is regarded as the most important aspect determining the feasibility of a specific process. Titanium dioxide is considered as an efficient semiconductor photocatalyst, especially for environmental remediation applications,[10,11] since it is inexpensive, and thermally, chemically, and biologically stable [12]. The commercially available TiO_2-P25 (Degussa/Evonik) showed a high photocatalytic activity towards the decomposition of various organic pollutants,[13,14] and it is regarded as a benchmark photocatalyst. Nevertheless, predominant drawbacks upon its utilization for light-assisted synthetic processes/reactions are a low porosity, fast photo-induced charges recombination, and - a non-selective reactivity important for organic synthesis (JC: of course if we are thinking about "organic synthesis").

The design and development of efficient an drawback-free TiO_2-based catalysts is still an open and challenging topic, especially with emphasis on specific selective photo-oxidation processes,[15] where controllable adjustment of surface feature including the porosity, morphology, surface chemistry heterogeneity, and/or size of particles showed to have a determinantal impact on the photoreactivity, as also architected morphologies have (JC: Please check).[15] Mechanochemistry applied as a synthetic tool brings an advantage of altering and tuned surface features on demand.[15–17] We have recently shown that the ultrasound-treatment of TiO_2-P25 in a basic medium led to the external surface's hydroxylation and had a positive impact on the porosity development and surface chemistry heterogeneity, resulting in an enhanced photocatalytic performance.[14] Our latest recent research efforts have been focused on new synthetic routes' development by employing

sonochemistry as a supplementary process intensification tool towards nanostructured TiO_2 of elevated photoreactivity.[18] Since the first pioneer reports of Neppira (1980, acoustic cavitation phenomenon),[19] and of Makino *et al.* in (1982, formation of free radicals upon water sonolysis),[20,21] ultrasonication has been inspiring the scientists as an unique source of power. The resulted physical, chemical, and optical effects of ultrasound irradiation are the results of the acoustic cavitation phenomenon. The harsh expansion and implosion of the cavitation can lead to the formation of localized hotspots, with temperature and pressure reaching up to 5000 ^{o}C and 1000 bars, respectively,[2,17,22] various chemical (reactive oxygen species and free radicals formation), mechanical (de-aggregation, improved mass transfer/diffusion, de-passivation, or acoustic streaming), and optical/sonoluminescence effects.[23–27] These effects can lead to unique and novel crystallization processes/pathways during the synthesis.

Ultrasound-assisted synthesis

Herein, we present a low-power high-frequency (500 kHz) ultrasound-assisted precipitation protocol (LPHFUS), that led to a unique nano-structured material with a superior performance as a heterogeneous photocatalyst both in gaseous and liquid phases. The main goals of our catalyst design was to avoid the energy demanding step of calcination, and to utilize the organic residues in order to increase chemical heterogeneity towards enhanced light absorption and photoreactivity, either in a gaseous phase against toxic vapors of chemical warfare agents (a mustard gas surrogate), or in a liquid phase, for selective oxidation of benzyl alcohol, a model lignin-biomass derived compound.[28] For the synthesis, a strongly basic aqueous solution (M?? NaOH) was placed inside a cup horn sonicator/reactor. Under ultrasonication (500 kHz) and stable temperate (60 ^{o}C), titanium isopropoxide in isopropanol solution (1:3 volumetric ratio) was added with a controllable rate (0.5 mL/min), followed by 10 min aging prior the filtration, washing, and drying (80 ^{o}C,16 h).

The obtained bright white powder is referred to as USprec. For comparison commercial TiO_2-P25 was tested.

Results and Discussion

CHARACTERIZATIONS - 883

The TEM images of USprec (Figure 1) show aggregates of spherical-like nanoparticle with sizes s from ~20 to 150 nm. They consist of different areas (sub-nanoparticles) with sizes between 4-7 nm, in which two lattices are distinguished. Considering the crystal spacing and the angles between the spacing, the detected lattice fringes distances are indexed to anatase phase.[29] Interestingly, an amorphous phases, either in between the ultra-nano (JC: Do we agree to use it?) sized anatase phases or on the outer surface of the aggregates is also visible. Analysis of the **X-Ray diffraction** pattern (Figure 1g, Table s1) indicates that USprec consists of anatase,[30,31] with an average crystallite size of 4 nm. This is in agreement with the HR-TEM analysis and the sizes are among the smallest ones reported in the literature.[14] Although, we should not exclude the existence of amorphous phases, not detectable by XRD, that can be suggested due to the low intensity and broadness of the peaks. The P25 consists of two polymorphs/phases, anatase (87±3 %) and rutile, with the crystallinity size (JC: crystalline) of the former to be 18 nm, more than four times higher than that in USprec, while of the size of rutile crustal is 25 nm. (JC: rephrase?)

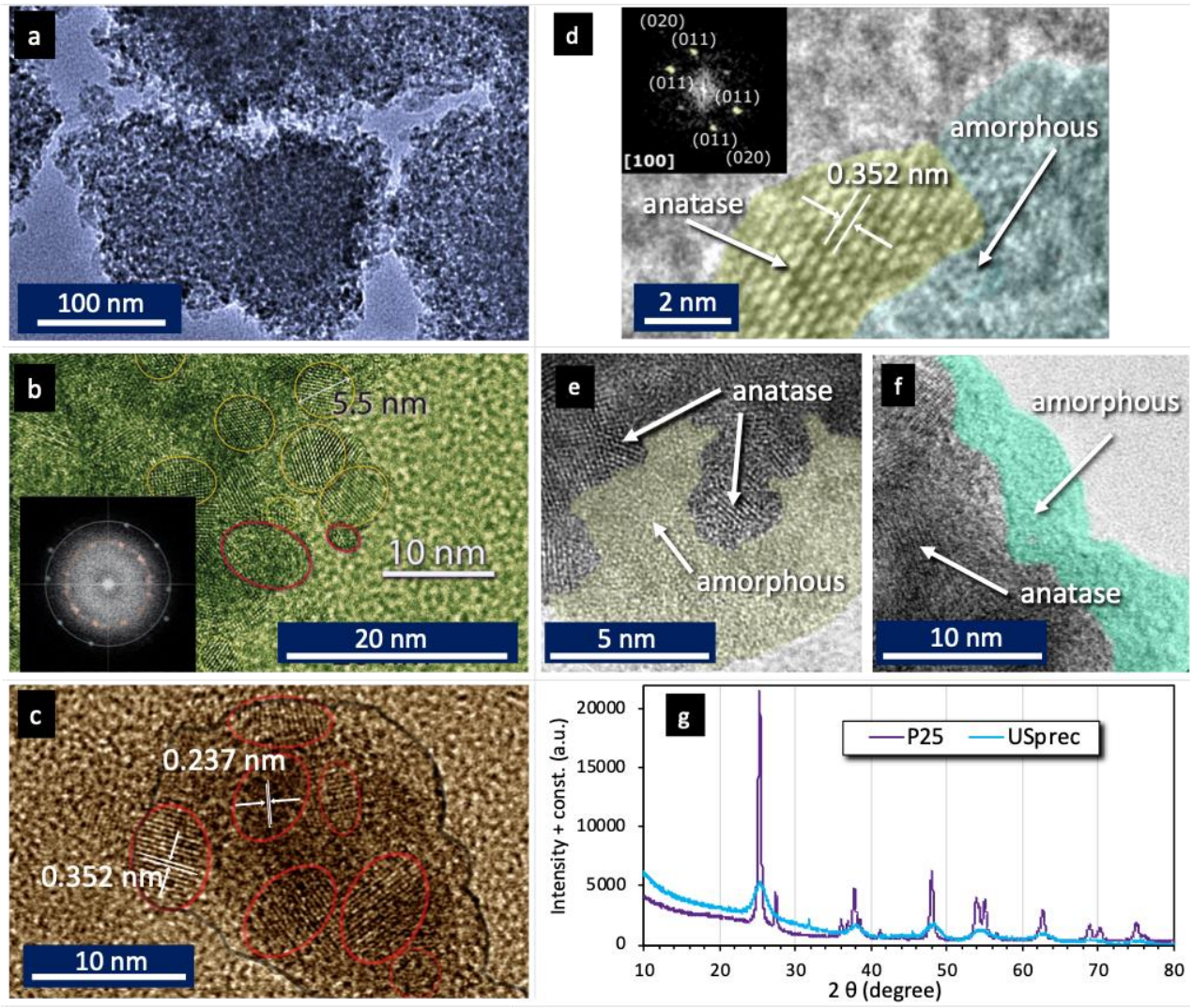

Figure 1. TEM and HR-TEM images of TiO_2 USprec (a-f), and the XRD patterns (g) for TiO_2 P25 and USprec.

Significant differences were also found in **textural features** (Table 1). The P25 isotherm (Type III, H3 hysteresis loop) revealed a mesoporous character of this materials with voids/interparticle spaces.[14,32] On the other hand, the isotherm of USprec showes a complex shape suggesting a mix micro-meso-porous nature.[32] Indeed, the micropores (1.2 to 1.7 nm) and mesopores (2.3 to 10.9 nm) are seen on its pore size distributions (PSD), with the latter consisting the ~89% of the total

pore volume (V_{Tot}=0.484 cm^3/g). The surface area of USprec is 326 m^2/g, which is 6 times higher than that of P25 and among the highest reported for spherical-like TiO_2 nanoparticles synthesized using template-free methods.[22,33] Surface areas in this range were reported predominately for TiO_2 amorphous phases (JC: Please remember we don't know how much amorphous phase we have, and this phase can be the reason for our high surface area…).[34]

The optical features were evaluated based on a **defuse reflectance** (DR) method in the UV-Vis-NIR range of light. The estimated optical band gaps (Figure 1g) are 3.2 and 3.3 eV for P25 and USprec, respectively, and they are in a good agreement with those reported in the literature for anatase (~3.2 eV).[35] The small difference can suggest a different photocatalytic behavior.

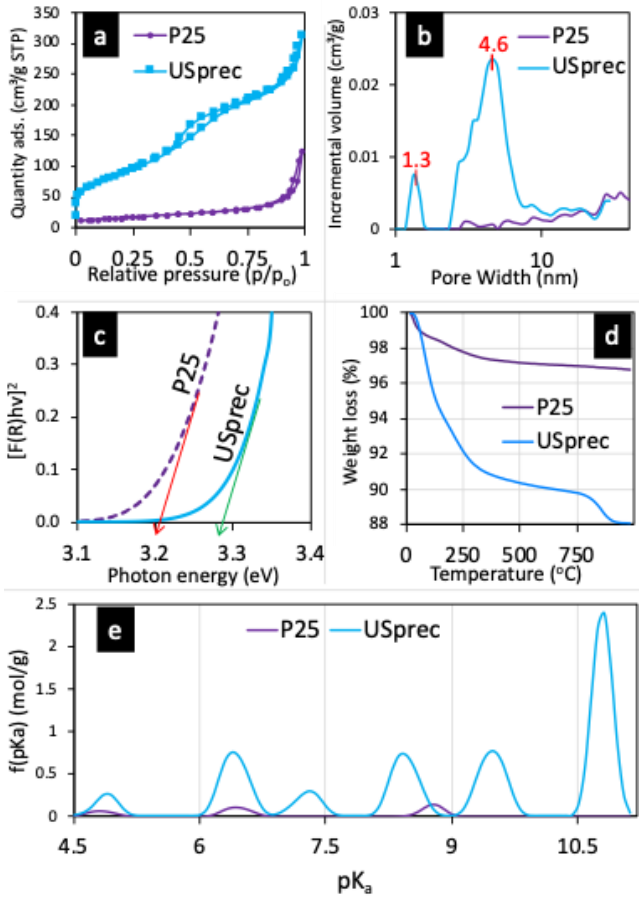

Figure 2. Nitrogen sorption isotherms (a), pores size distribution based on NLDFT method (b), Tauc plots derived from defuse reflectance UV-Vis-NIR absorption spectra using the Kubelka-Munk function (c), the thermal gravimetry curves in air (d) and the distribution of the surface functional group (e) for TiO_2 P25 and USprec.

Since our synthesis protocol targeted also the development of TiO_2 chemical heterogeneity to increase its photocatalytic activity, the surface chemistry was evaluated in details. **ATR-FTIR** spectrum (Figure s4) for USprec revealed that the bands linked to Ti-O-Ti bonds have a lower intensity than those on the P25 spectrum, and the ones linked to -OH and C-containing groups are more intense.[14,30] Additionally, the small shoulder between 880-1020 cm^{-1} is linked to Ti-OH or/and Ti-O-C moieties.[14] The results of the **thermal analysis** (TA) in air showed that up to 1000 ^oC, P25 lost 3.3% weight and USprec-12 %, suggesting a more complex and less thermally stable chemical composition of the latter sample. To further investigate the surface decomposition upon heat treatments, TA was performed in **helium** and the off-gases were analyzed by mass spectroscopy (MS). The MS thermal profiles of the m/z representing H_2O/OH, C, CH_3, and CO_2 (Figure s6) indicated that the higher weight loss in the case of USprec is related to the removal/decomposition of water and oxygen or/and carbon containing moieties, such as -OH, -C-O, -COO, and -C=O. (JC: all components of the material are very important, including the "organic component": The crucial element of this publication is the perfectly explain (with some evidence) how those component were formed during the synthesis and how they are interacting within the composite material…then the photocatalytic activity is "easy" to explain…I know: having no too much space in Nature Materials to explain that is very challenging…)

The **pK_a distributions** of the surface functional groups (SFGs) (Figure s8) of P25 revealed two species of a pK_a<7, assigned to bridging and acidic terminal oxygen containing functionalities, and one with pK_a>7 - to basic terminal hydroxyl groups.[14,36,37] The presence of six SFGs on USprec indicates a high degree surface chemical heterogeneity. The density of SFGs per unit surface area ($d_{SFGs/SA}$) is 2.1 and 5.8 μmol/m^2 for P25 and USprec, respectively. Interestingly, for USprec mainly basic SFGs contribute to that high density , since the densities of species with pK_a<7 are equivalent.

While the **X-ray photoelectron spectroscopy** (XPS) spectra of **Ti 2*p*$_{3/2}$**, showed only Ti-O-Ti on P25, the contribution of these bonds for USprec was only 17.6 % for USprec, with the rest of Ti^{4+} assigned either to Ti-OH and Ti-O-C bonds or to defects.[14,38,39] Similar results were reported for black titania and for ultrasound treated TiO_2, linked to hydrogenation of Ti-O to Ti-H and Ti-OH.[14,40] The deconvolution of **C 1*s*** spectrum of USprec revealed the presence of C-O, C=O, O-C=O or/and hydrocarbonate.[41–44] The contribution of adventitious carbon was much lower on USprec than that on P25, which supports our hypothesis that the residue from the organic precursors is incorporated to the surface/matrix of USprec. The main contribution of the **O 1*s*** core energy level spectrum of P25 is linked to Ti-O-Ti (84.1%) and the rest to Ti-O-H. For USprec, the predominant contributions are hydroxyl groups (82.9% both together) and ester or alkoxy oxygen (17.1%). This suggests that organic residue from the precursors was oxidized either to carboxylate or carbonates.[41,42] These results are in a good agreement with the PT results, which indicated a high density of surface functional groups on USprec, especially with pK_a>7.

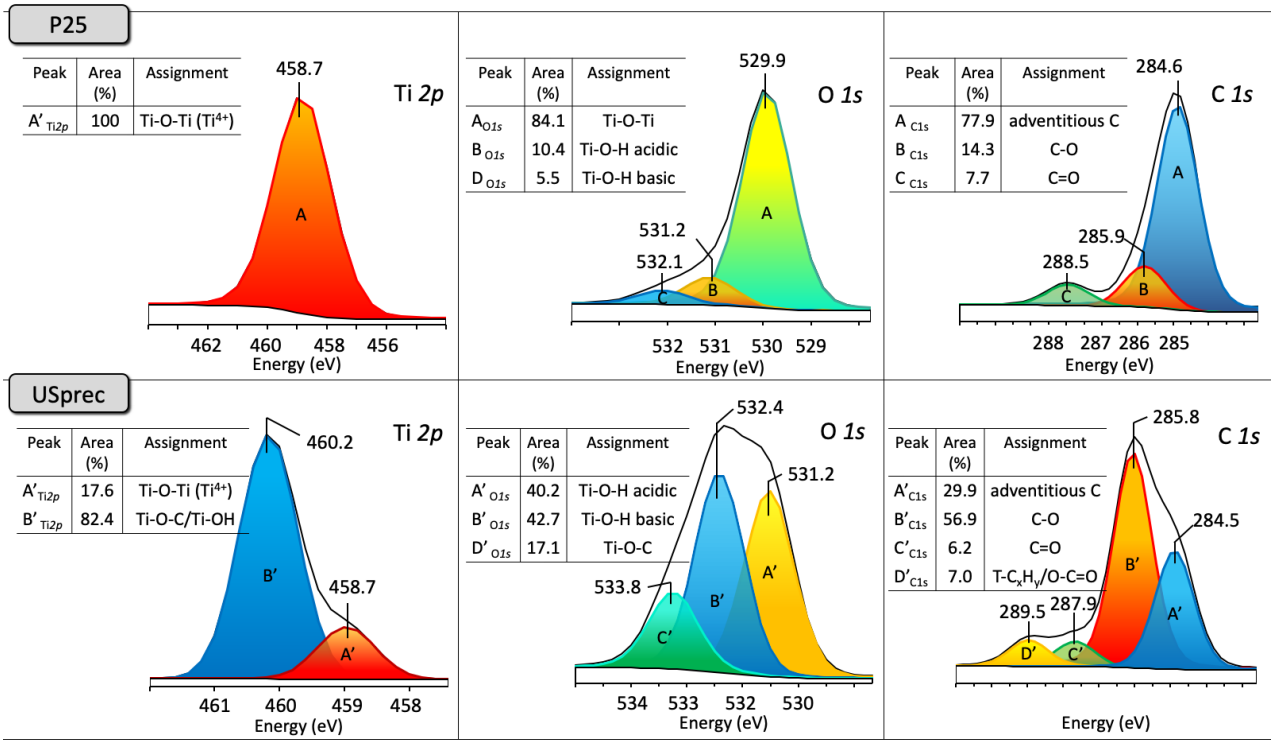

Figure 3. XPS high-resolution deconvoluted core energy level spectra of Ti $2p_{3/2}$, O *1s*, and C *1s*.

CRYSTALIZATION MECHANISM-534

The crystallization can undergo via various pathways like alkoxolation, oxolation, olation, alcoholic permutation, hydrolysis, and condensation reactions.[45] These alternative reactions are competitive, and the most influential factors are the initially formed hydroxo-aquo precursors $[Ti(OH)_x(OH_2)_{6-x}]^{(4-x)+}$, the amount of the water (involved directly to the hydrolysis), and physicochemical parameters such as pH and temperature. Under ultrasonication, the formation of the cavitation/hot-spot plays a key role, since isopropanol can diffuse inside the cavitation/bubble (lower boiling point compared to water), promoting the rapid removal of the organic residues and the fast nucleation/growth of the anatase phase at the cavity's interfacial zone via the oxolation reaction (Figure X), due to the high temperature and pressure.[46] The further collapse of the

isopropanol-containing cavitation favors the polymerization/polycondensation of the $Ti(OH)_4$ phase,[47] surrounding the TiO_2 crystals via the olation reaction (Figure X),[48] while organic residues remained either at the surface of the TiO_2 nanocrystals or/and at the formed amorphous titanium hydroxide phase. The formation of the latter phase can be promoted by the high pH and by the hydroxyl radicals formed in ultrasonic-driven process.[49]

Considering all the above, we concluded that nanosized TiO_2 oligomers/crystals/particles of anatase (4-7 nm in size) were initially formed (Figure 4), and an amorphous in nature titanium hydroxide layer was formed around them, blocking the further growth of the anatase phase. The presence of residues (JC: Do you mean "organic residues"?) prevented the continuous crystallization, promoting also the formation of the amorphous/hydroxylated phases, and preventing the interparticle agglomeration.[33] The nanosized anatase crystals were cross-linked with an amorphous phase creating a continuous network in which voids/cages/mesopores exist. Their creation can be assigned also to the interparticle spaces between the well-crystalized nanoparticles. That amorphous phase can also be responsible for the high porosity and high degree of the surface chemical heterogeneity of USprec. The formation of a dual phase nanomaterial containing a residual organic phase and TiO_2 in our synthesis process (Figure 4) could be of paramount importance in catalysis. The organic phase origin is in non-reacted isopropoxide or/and the alcohol molecules interacted with the inorganic phases (JC: Please remember that we are working under such specific "500kHz-US + NaOH + others" conditions). The applied conditions affected markedly its chemistry.

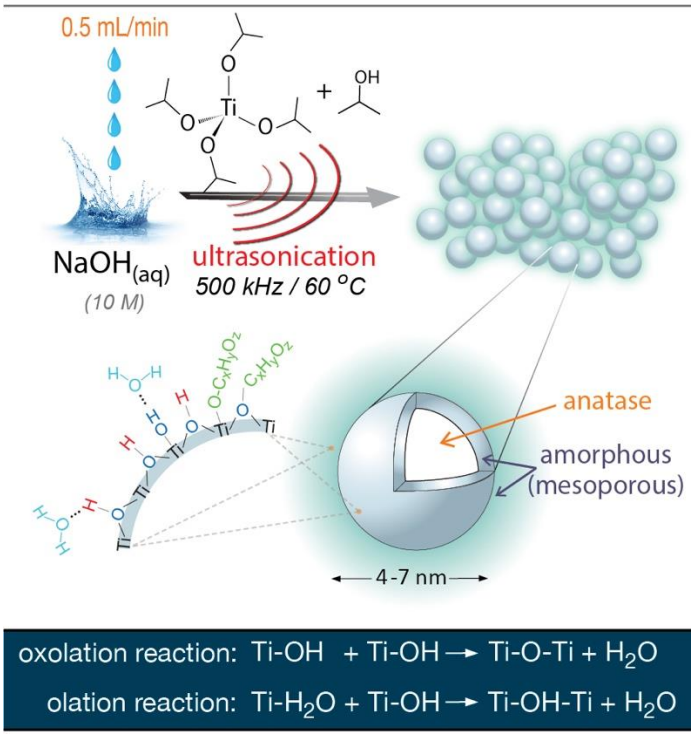

Figure 4. AAAAAaaa

Anatase is more photoactive than other polymorphs, like rutile,[50] while the co-presence of two phases in intimate contact has a beneficial effect on the photoreactivity, by promoting the photogenerated electron and hole pairs' separation.[51] In the case of anatase-rutile interfaces, the separation of e^-/h^+ was linked to the differences in valence and conduction energy levels, with the holes flow towards rutile and electrons towards anatase.[52] Krylova et al. showed that in a core-shell-like structures consisting of a rutile shell and an amorphous core, the electrons can migrate to the core from the shell, due to the higher electron affinity of the former since the covalent band position of the amorphous phase is lower than that of rutile.[50] Hole, on the contrary, migrate from core to shell , since the valence band of rutile is higher compared to the one of the amorphous one. A high photoreactivity of USpres was expected, not only due to the presence of the two phases in contact and their favorable band gap alignments, but also as a result of the carbon containing

phases, that can act as “antenna/photosensitizers” elevating the photon absorption (JC: but pure USprec is not showing any absorption in visible (DR UV-vis characterization)).

CATALYTIC RESULTS – 622 words

USprec and P25 were evaluated as photo-detoxifiers of toxic vapors, and specifically of 2-chloroethyl ethyl sulfide (CEES, $CH_3CH_3SCH_2CH_2Cl$), a surrogate of the chemical warfare agent mustard gas. The experiments were run either under light irradiation (visible or ultraviolent) or in the dark for various exposure times. Two aspects/factors were evaluated: the adsorptive detoxification and the reactive/catalytic one, since both are desirable features for the targeted application. The former aspect was evaluated based on the weight uptake expressed per gram of the catalyst (WU) in the dark (Figure 5a), with USprec showing WUs of 209 and 424 mg/g after 1- and 7-days of exposure, respectively. These values were 3 and 2.4 times higher than those of P25. The comparison with other materials tested under the same conditions (Figure 5b) disclosed that USprec outperformed various efficient nanostructures reported in the literature, such as ultrasound-treated hydroxylated P25 (P25-US) and even its composite with reduced graphite oxide, $BaTiO_x$ (size ~20nm), ZnO_2, and $Zr(OH)_4$ nanoparticles.[14,36,53,54] Desorption tests revealed a superior strength of adsorption on USprec, since after 1 and 7 day exposure in the dark sample were left under ambient conditions, the remaining weights of the adsorbed quantities were 93 and 54 %, respectively. For P25, these values were only 21 and 16 %.

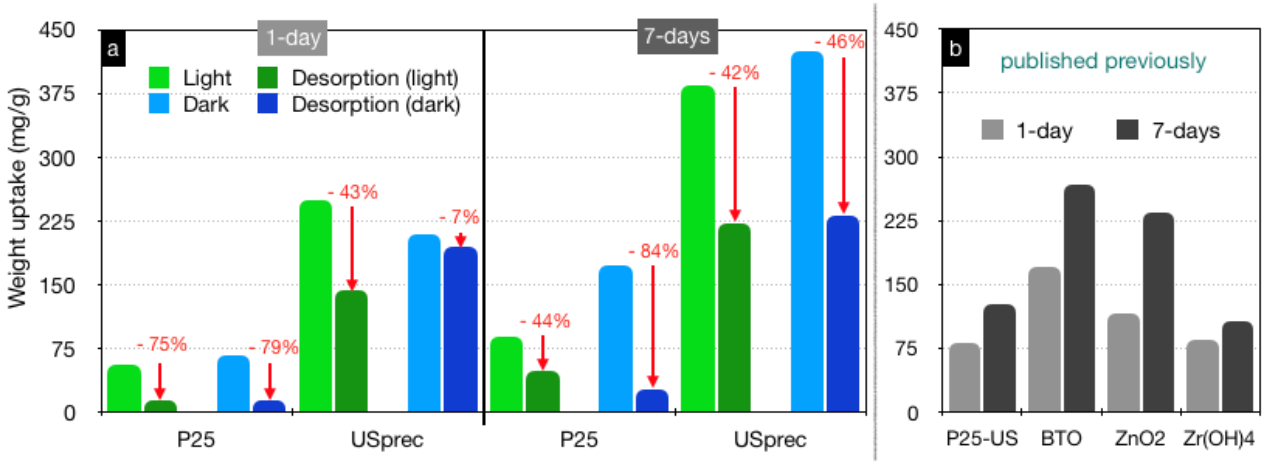

Figure 5. Weight uptakes for TiO_2 P25 and USprec with the red arrows representing the extent of the desorption effect (a) and data reported in the literature for other materials evaluated at the same conditions (hydroxylated P25, barium titanate nanoparticles (BTO), zinc peroxide nanoparticles (ZnO_2), and zirconium hydroxide [14,36,53,54]).

For USprec, the WUs after 1- and 7-days exposure under visible light irradiation (Figure 5b) were 245 and 385 mg/g, respectively, and significantly higher than those for P25. To withdraw specific conclusions based only on the comparison under light and in the dark is a complex task, since the light irradiation does not exclude simultaneous physical adsorption and photo-driven catalytic decomposition processes, that can lead to plenty of compounds which can be either strongly retained on the surface or be volatilized. The extent of the volatiles formation can be detected based on the desorption tests on the 1-day exposed samples. For USprec, when the adsorption and desorption were performed in the dark, the amount adsorbed decreased only 7 %, while that under visible light- 43 %. Under ultraviolet irradiation (UV) for 7-days, the WUs for P25 and USprec were 174 and 370 mg/g, respectively. This further supports the higher photo-detoxification capability of USprec compared to that of P25.

Analysis of the headspaces of the closed vials and of the acetonitrile extracts of the spent materials **was performed** by **GC-MS and all** chromatograms and their detailed analyses are collected in the Supplementary Information (Figure s9-s11). The formed products and the involved mechanisms are summarized in Figure X. The elevated surface reactivity of USprec is supported by its high activity to hydrolyze CEES to hydrolyl ethyl ethyl sulfide (HEES) even in the dark. The most significant finding is the detection of non-sulfur oxygen containing molecules as a result of radicals' reactions and **photo-driven--oxidation**. These processes resulted in the formation/detection of acetaldehyde (MeCHO), chloro-acetaldehyde (Cl-MeCHO), and acetic acid (AcOH). The latter reacted further with formed radicals leading to esters, ethyl- (EtOAc) and methyl-acatate (MeOAc). This process took place on only in the presence of USprec, supporting the higher photoreactivity than that of P25. Additionally, disulfides (diethyl disulfide (DEDS), bis(2-chloroethyl) disulfide (b2CEDS), and 2-chloroethyl ethyl disulfide (2CEEDS)) were formed and 2CEEDS appeared even under visible/ambient light. It is very important to point out that the formation of b2CEDS is rarely reported in the literature and that the products of a higher toxicity than that of CEES (like sulfones) were not formed. Moreover, the formation of disulfides is considered as a desirable process, since due to their high boiling points, they remain adsorbed on the surface, and were detected only in the extracts. For environmental remediation-oriented applications, the photocatalyst's ability to completely un-selectively decompose/degrade the pollutants is an important asset. On the contrary, for synthetic chemistry application, the selective conversion is the ultimate goal.

BnOH - 236 words

The high **photo-oxidation** activity of USprec driven us to study also its suitability as heterogeneous photocatalysts in a liquid phase for the selective partial oxidation of a value-added

platform compound, benzyl alcohol (BnOH), that can be derived from abundantly and naturally available lignocellulosic biomass.[4,55,56] Details regarding the optimization of the photocatalysis tests are in the Supplementary Information and elsewhere.[18,28] The results presented in Figure 6 showed an almost 100 % conversion of BnOH on P25, and 61 % on USprec. Moreover the selectivity of benzyl alcohol (PhCHO) on USprec was 100 % and on P25 only 41%. It is important to mention that, P25 decomposed/mineralized the formed benzyl aldehyde, since the aromatic balance was only 40% (no other compounds as benzoic acid or aliphatic ones were detected). This extent of the activity is an undesired feature of synthetic photochemistry. On the other hand, on USprec, both the selectivity and yield of PhCHO by partial photo-oxidation of BnOH were 100% and the formed product was not further oxidized or degraded. The ~~ultra~~nanosize of USprec and the high density of its hydroxyl as well as of the carbon containing groups could be regarded as the activity governing factors as introducing various interfacial processes different from those on the commercial pure oxide phase. Leaching tests after the photocatalytic tests were performed in all cases, and no Ti species were detected, revealing the stability of this material during these tests.

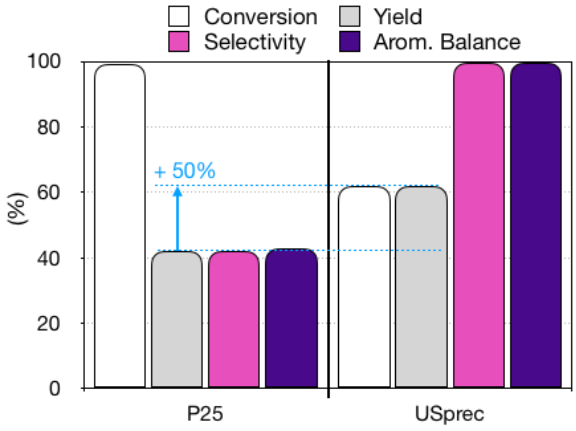

Figure 6. Benzyl alcohol (1 mM in acetonitrile) oxidation to benzyl aldehyde under ultraviolet irradiation (365 nm, power 450 mW) at 30 ^{o}C for 6 hours.

I really think we need to propose a hypotheis on the photoactivity….. I proposed that pseudochromphores, but if you ahv any idea, lets dicuss it. Otherwise band gap shows that materials aer not photoactive in visible..

Conclusions

In summary, the herein presented and discussed results showed how mechanochemistry can be utilized as a "green" synthetic tool of a design and synthesis of novel nanocatalysts. The followed low-power high-frequency (500 kHz) ultrasound-assisted precipitation synthesis (LPHFUS) resulted in a novel multiphase nano-structured titanium dioxide with elevated textural and surface chemistry features, crucial for catalytic applications. The energy consuming step of calcination towards crystallization was avoided, while the organic residues played a crucial role not only in the material synthesis but also in its photoactovity (JC: I suggest to highlight that the synthesis is "very short" (process intensification) due to "500kHz US"). This nanomaterial showed a superior performance as heterogenous photocatalyst either for environmental remediation application such as detoxification of toxic vapors and for biomass valorization through selective photooxidation.

The elevated surface heterogeneity of USprec can be associated to its small size of the nanoparticles, the developed porosity, the surface hydroxylation, and the presence of various C-containing SFGs.

Acknowledgments

DAG, DL, and JCC would like to acknowledge the support from the National Science Centre in Poland within OPUS-13 project nr 2017/25/B/ST8/01592 (http://photo-catalysis.org). DAG is very grateful for the support from National Science Centre of Poland, providing the opportunity to perform part of the experiments in the City College of New York, City University of New York (USA) within the frame of the scientific activity grant Miniatura 2 (registration number 2018/02/X/ST5/03531).

References

1. FUJISHIMA, A. & HONDA, K. Electrochemical Photolysis of Water at a Semiconductor Electrode. *Nature* **238**, 37–38 (1972).
2. Colmenares Q., J. C. Ultrasound and Photochemical Procedures for Nanocatalysts Preparation: Application in Photocatalytic Biomass Valorization. *J. Nanosci. Nanotechnol.* **13**, 4787–4798 (2013).
3. Chatel, G., Valange, S., Behling, R. & Colmenares, J. C. A Combined Approach using Sonochemistry and Photocatalysis: How to Apply Sonophotocatalysis for Biomass Conversion? *ChemCatChem* **9**, 2615–2621 (2017).
4. Colmenares, J. C. *et al.* Nanostructured photocatalysts and their applications in the photocatalytic transformation of lignocellulosic biomass: An overview. *Materials (Basel).* **2**, 2228–2258 (2009).
5. Colmenares, J. C. & Luque, R. Heterogeneous photocatalytic nanomaterials: prospects and challenges in selective transformations of biomass-derived compounds. *Chem. Soc. Rev.* **43**, 765–778 (2014).
6. Zhou, T., Wu, X., Mao, J., Zhang, Y. & Lim, T.-T. Rapid degradation of sulfonamides in a novel heterogeneous sonophotochemical magnetite-catalyzed Fenton-like (US/UV/Fe3O4/oxalate) system. *Appl. Catal. B Environ.* **160**–**161**, 325–334 (2014).
7. Barndõk, H. *et al.* Degradation of 1,4-dioxane from industrial wastewater by solar photocatalysis using immobilized NF-TiO2 composite with monodisperse TiO2 nanoparticles. *Appl. Catal. B Environ.* **180**, 44–52 (2016).
8. Dionysiou, D. D., Suidan, M. T., Bekou, E., Baudin, I. & Laîné, J. M. Effect of ionic strength and hydrogen peroxide on the photocatalytic degradation of 4-chlorobenzoic acid in water. *Appl. Catal. B Environ.* **26**, 153–171 (2000).
9. Anipsitakis, G. P. & Dionysiou, D. D. Transition metal/UV-based advanced oxidation technologies for water decontamination. *Appl. Catal. B Environ.* **54**, 155–163 (2004).
10. Friedmann, D., Mendive, C. & Bahnemann, D. TiO2 for water treatment: Parameters affecting the kinetics and mechanisms of photocatalysis. *Appl. Catal. B Environ.* **99**, 398–406 (2010).
11. Shahadat, M., Teng, T. T., Rafatullah, M. & Arshad, M. Titanium-based nanocomposite materials: A review of recent advances and perspectives. *Colloids Surfaces B Biointerfaces* **126**, 121–137 (2015).
12. Wu, C. Y., Tu, K. J., Lo, Y. S., Pang, Y. L. & Wu, C. H. Alkaline hydrogen peroxide treatment for TiO2 nanoparticles with superior water-dispersibility and visible-light photocatalytic activity. *Mater. Chem. Phys.* **181**, 82–89 (2016).
13. Ohtani, B., Prieto-Mahaney, O. O., Li, D. & Abe, R. What is Degussa (Evonic) P25? Crystalline composition analysis, reconstruction from isolated pure particles and photocatalytic activity test. *J. Photochem. Photobiol. A Chem.* **216**, 179–182 (2010).
14. Giannakoudakis, D. A. *et al.* Ultrasound-activated TiO2/GO-based bifunctional photoreactive adsorbents for detoxification of chemical warfare agent surrogate vapors. *Chem. Eng. J.* **395**, 125099 (2020).
15. Giannakoudakis, D. A., Chatel, G. & Colmenares, J. C. Mechanochemical Forces as a Synthetic Tool for Zero- and One-Dimensional Titanium Oxide-Based Nano-photocatalysts. *Top. Curr. Chem.* **378**, 2 (2020).

16. Ouyang, W. *et al.* Mechanochemical Synthesis of TiO2 Nanocomposites as Photocatalysts for Benzyl Alcohol Photo-Oxidation. *Nanomaterials* **6**, 93 (2016).
17. Chatel, G. & Colmenares, J. C. Sonochemistry: from Basic Principles to Innovative Applications. *Top. Curr. Chem.* **375**, 8 (2017).
18. Pradhan, S. R., Nair, V., Giannakoudakis, D. A., Lisovytskiy, D. & Colmenares, J. C. Design and development of TiO2 coated microflow reactor for photocatalytic partial oxidation of benzyl alcohol. *Mol. Catal.* **486**, 110884 (2020).
19. Neppiras, E. A. Acoustic cavitation. *Phys. Rep.* **61**, 159–251 (1980).
20. Makino, K., Mossoba, M. M. & Riesz, P. Chemical effects of ultrasound on aqueous solutions. Evidence for hydroxyl and hydrogen free radicals (.cntdot.OH and .cntdot.H) by spin trapping. *J. Am. Chem. Soc.* **104**, 3537–3539 (1982).
21. Makino, K., Mossoba, M. M. & Riesz, P. Chemical effects of ultrasound on aqueous solutions. Formation of hydroxyl radicals and hydrogen atoms. *J. Phys. Chem.* **87**, 1369–1377 (1983).
22. Yu, J. C., Yu, J., Ho, W. & Zhang, L. Preparation of highly photocatalytic active nano-sized TiO2 particles via ultrasonic irradiation. *Chem. Commun.* **d**, 1942–1943 (2001).
23. Magdziarz, A. & Colmenares, J. C. In situ coupling of ultrasound to electro-and photo-deposition methods for materials synthesis. *Molecules* **22**, (2017).
24. Cravotto, G. & Cintas, P. Harnessing mechanochemical effects with ultrasound-induced reactions. *Chem. Sci.* **3**, 295–307 (2012).
25. Pokhrel, N., Vabbina, P. K. & Pala, N. Sonochemistry: Science and Engineering. *Ultrason. Sonochem.* **29**, 104–128 (2016).
26. Berlan, J., Trabelsi, F., Delmas, H., Wilhelm, a. M. & Petrignani, J. F. Oxidative degradation of phenol in aqueous media using ultrasound. *Ultrason. Sonochem.* **1**, S97–S102 (1994).
27. Suslick, K. S., Hammerton, D. A. & Cline, R. E. The Sonochemical Hot Spot. *J. Am. Chem. Soc.* **108**, 5641–5642 (1986).
28. Giannakoudakis, D. A., Łomot, D. & Colmenares, J. C. When sonochemistry meets heterogeneous photocatalysis: designing a Sonophotoreactor towards sustainable selective oxidation. *Green Chem.* (2020). doi:10.1039/d0gc00329h
29. Zhang, K. *et al.* An order/disorder/water junction system for highly efficient co-catalyst-free photocatalytic hydrogen generation. *Energy Environ. Sci.* **9**, 499–503 (2016).
30. Tan, L.-L., Ong, W.-J., Chai, S.-P. & Mohamed, A. Reduced graphene oxide-TiO2 nanocomposite as a promising visible-light-active photocatalyst for the conversion of carbon dioxide. *Nanoscale Res. Lett.* **8**, 465 (2013).
31. Viriya-empikul, N. *et al.* Effect of preparation variables on morphology and anatase-brookite phase transition in sonication assisted hydrothermal reaction for synthesis of titanate nanostructures. *Mater. Chem. Phys.* **118**, 254–258 (2009).
32. Thommes, M. *et al.* Physisorption of gases, with special reference to the evaluation of surface area and pore size distribution (IUPAC Technical Report). *Pure Appl. Chem.* **87**, 1051–1069 (2015).
33. Teh, C. Y., Wu, T. Y. & Juan, J. C. An application of ultrasound technology in synthesis of titania-based photocatalyst for degrading pollutant. *Chemical Engineering Journal* **317**, 586–612 (2017).
34. Li, W. *et al.* Template-free synthesis of uniform magnetic mesoporous TiO 2 nanospindles for highly selective enrichment of phosphopeptides. *Mater. Horizons* **1**, 439–445 (2014).
35. Gupta, S. M. & Tripathi, M. A review of TiO2 nanoparticles. *Chinese Sci. Bull.* **56**, 1639–1657 (2011).
36. Giannakoudakis, D. A., Mitchell, J. K. & Bandosz, T. J. Reactive adsorption of mustard gas surrogate on zirconium (hydr)oxide/graphite oxide composites: the role of surface and chemical features. *J. Mater. Chem. A* **4**, 1008–1019 (2016).
37. Giannakoudakis, D. A., Arcibar-Orozco, J. A. & Bandosz, T. J. Effect of GO phase in Zn(OH)2/GO composite on the extent of photocatalytic reactive adsorption of mustard gas surrogate. *Appl. Catal. B Environ.* **183**, 37–46 (2016).
38. Ren, W. *et al.* Low temperature preparation and visible light photocatalytic activity of mesoporous carbon-doped crystalline TiO2. *Appl. Catal. B Environ.* **69**, 138–144 (2007).
39. Wu, Z. *et al.* The fabrication and characterization of novel carbon doped TiO 2 nanotubes, nanowires and nanorods with high visible light photocatalytic activity. *Nanotechnology* **20**, (2009).
40. Hamad, H. *et al.* Synthesis of TixOynanocrystals in mild synthesis conditions for the degradation of pollutants under solar light. *Appl. Catal. B Environ.* **241**, 385–392 (2019).
41. Guo, J. *et al.* The preparation and characterization of a three-dimensional titanium dioxide nanostructure

with high surface hydroxyl group density and high performance in water treatment. *Chem. Eng. J.* **221**, 342–352 (2013).
42. Zhu, J. *et al.* Nanocrystalline anatase TiO2 photocatalysts prepared via a facile low temperature nonhydrolytic sol-gel reaction of TiCl4 and benzyl alcohol. *Appl. Catal. B Environ.* **76**, 82–91 (2007).
43. Ai, Z., Wu, N. & Zhang, L. A nonaqueous sol-gel route to highly water dispersible TiO2 nanocrystals with superior photocatalytic performance. *Catal. Today* **224**, 180–187 (2014).
44. Yang, C. *et al.* Rational design of carbon-doped TiO2 modified g-C3N4 via in-situ heat treatment for drastically improved photocatalytic hydrogen with excellent photostability. *Nano Energy* **41**, 1–9 (2017).
45. Livage, J., Henry, M. & Sanchez, C. Sol-gel chemistry of transition metal oxides. *Prog. Solid State Chem.* **18**, 259–341 (1988).
46. Ghows, N. & Entezari, M. H. Ultrasound with low intensity assisted the synthesis of nanocrystalline TiO2 without calcination. *Ultrason. Sonochem.* **17**, 878–883 (2010).
47. Huang, W., Tang, X., Wang, Y., Koltypin, Y. & Gedanken, A. Selective synthesis of anatase and rutile via ultrasound irradiation. *Chem. Commun.* 1415–1416 (2000). doi:10.1039/b003349i
48. Zhang, J. *et al.* The formation mechanism of TiO2 polymorphs under hydrothermal conditions based on the structural evolution of [Ti(OH)h(H2O)6-h]4-h monomers. *J. Mater. Chem. C* **7**, 5764–5771 (2019).
49. Lee, G. H. & Zuo, J.-M. Growth and Phase Transformation of Nanometer-Sized Titanium Oxide Powders Produced by the Precipitation Method. *J. Am. Ceram. Soc.* **87**, 473–479 (2009).
50. Krylova, G. & Na, C. Photoinduced Crystallization and Activation of Amorphous Titanium Dioxide. *J. Phys. Chem. C* **119**, 12400–12407 (2015).
51. Florent, M., Giannakoudakis, D. A. & Bandosz, T. J. Detoxification of mustard gas surrogate on ZnO2/g-C3N4 composites: Effect of surface features' synergy and day-night photocatalysis. *Appl. Catal. B Environ.* **272**, 119038 (2020).
52. Scanlon, D. O. *et al.* Band alignment of rutile and anatase TiO2. *Nat. Mater.* **12**, 798–801 (2013).
53. Giannakoudakis, D. A. *et al.* Barium titanate perovskite nanoparticles as a photoreactive medium for chemical warfare agent detoxification. *J. Colloid Interface Sci.* **531**, 233–244 (2018).
54. Giannakoudakis, D. A. *et al.* Zinc peroxide nanoparticles: Surface, chemical and optical properties and the effect of thermal treatment on the detoxification of mustard gas. *Appl. Catal. B Environ.* **226**, 429–440 (2018).
55. Nitsos, C. K., Matis, K. A. & Triantafyllidis, K. S. Optimization of hydrothermal pretreatment of lignocellulosic biomass in the bioethanol production process. *ChemSusChem* **6**, 110–122 (2013).
56. Giannakoudakis, D. A. *et al.* Additive-free photo-assisted selective partial oxidation at ambient conditions of 5-hydroxymethylfurfural by manganese (IV) oxide nanorods. *Appl. Catal. B Environ.* **256**, 117803 (2019).